ChemComm

ROYAL SOCIETY OF CHEMISTRY

COMMUNICATION

View Article Online
View Journal | View Issue

Cite this: *Chem. Commun.*, 2026, **62**, 5447

Received 2nd January 2026,
Accepted 11th February 2026

DOI: 10.1039/d6cc00016a

rsc.li/chemcomm

Conformation-driven (de)localization of the exciton in 2-phenylpyridine oligomers: non-adiabatic surface hopping dynamics

Palak Mandal and Aditya N. Panda *

We report on non-adiabatic surface-hopping dynamics of exciton localization and delocalization processes in two 2-phenylpyridine oligomers: a linear and a helical one. In the linear pentamer, excited-state relaxation involves the delocalization of the exciton across multiple monomer units. In contrast, the relaxation in the helical pentamer proceeds with the localization of the exciton on a single monomeric unit.

In recent years, conjugated oligomers and polymers have attracted considerable interest for their potential applications in organic electronic devices, primarily due to their unique optoelectronic properties.[1–3] Organic material-based electronic devices have many advantages over their inorganic counterparts, such as low cost, lightweight, and mechanical flexibility. However, in terms of performance and efficiency, these organic material-based electronic devices are not as good as compared to inorganic devices.[4–7] The efficiency of these devices depends on various photo-induced dynamics processes, such as charge and energy transfer, charge separation and recombination, localization and delocalization of excitons, *etc.*[8–12] These processes in large conjugated systems are greatly affected by their distinct geometrical architectures.[13–15] For example, the extent of exciton delocalization after photo-excitation in π-conjugated oligomers, such as oligophenylene and oligothiophene, differs in different molecular conformers (linear *vs.* cyclic).[13,16] Therefore, a comprehensive understanding of molecular structure and its influence on the photo-induced dynamics process is essential for the effective design of suitable organic electronic devices.

Modeling the photo-induced processes mentioned above poses significant challenges, as it involves calculating the energies of multiple electronic states and the non-adiabatic coupling between them. In this regard, trajectory-based quantum–classical methods, such as Ehrenfest dynamics and trajectory surface hopping (TSH) dynamics,[17,18] have been useful for addressing the above issue. TSH is the most widely used method for simulating non-adiabatic dynamics, due to its simplicity, practicality, and scalability.[19] This method requires the calculation of electronic energies, gradients and couplings between excited states on-the-fly, which is computationally very intensive for larger conjugated systems, even when employing commonly used time-dependent density functional theory (TD-DFT) methods. In recent times, many semiempirical quantum methodologies have been developed to alleviate the problem of resources and time for larger systems.[13,20–22] In this context, the semiempirical time-dependent density functional tight binding (TD-DFTB) method, which is analogous to TD-DFT but employs parameterized integrals with smaller basis sets, has also become very useful.[23] In the past few years, photo-induced dynamics employing TSH with TD-DFTB have been studied for a large number of conjugated systems, including oligomers of phenylenes, and acene derivatives.[24–28]

Oligophenylene and its conformational isomers, such as *ortho*, *meta*, and *para*-oligophenylene, have long been studied due to their interesting optical and electronic properties.[29–33] However, recent studies have shown that the presence of electron-withdrawing pyridine rings in oligomers results in significant alterations in the electrochemical and optical properties compared to the homo-oligomeric forms.[34–37] This suggests that the introduction of pyridine rings into oligophenylenes may also lead to significant changes in their electronic and optical properties. In this work, we have considered two different conformers **A** and **B** of oligomers of 2-phenylpyridine (**PhPy**), shown in Fig. 1, to investigate how the excited states evolve after photoexcitation. This follows our previous study on the oligomers of **PhPy**,[38] which discussed the static excited state properties of three different conformers of oligomers. In conformer **A**, the oligomers are formed by connecting the *para*-position of the phenylene ring of one **PhPy** unit with the *meta*-position of the pyridine ring of another **PhPy** unit. On the other hand, the oligomers of conformer **B** are formed by connecting the *para*- and *ortho*-positions of the phenylene and pyridine rings of two different **PhPy** units, respectively. Conformer **A** remains linear as we move from

Department of Chemistry, Indian Institute of Technology Guwahati, Guwahati, India. E-mail: anp@iitg.ac.in

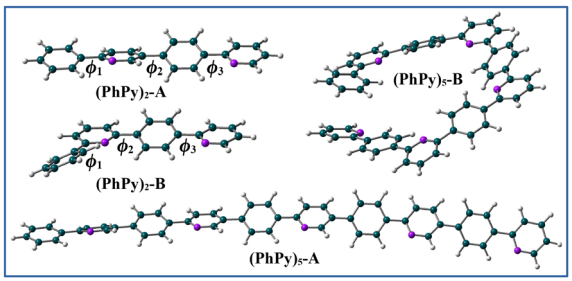

Fig. 1 Ground state optimized geometries of dimers and pentamers of conformers **A** and **B** obtained at the B3LYP-D3BJ/def2-TZVP level.

(PhPy)$_2$ to **(PhPy)$_5$**, while conformer **B** adopts a helical-like structure for **(PhPy)$_5$** (Fig. 1). The TSH dynamics was carried out in combination with the TD-DFTB method. In addition to TD-DFTB, the vertical excitation energies (E_g) are also calculated at the long-range corrected (LC) version of TD-DFTB (LC-TD-DFTB),[39,40] and these results are compared with the results obtained at the algebraic diagrammatic construction scheme to the second order (ADC(2)) level.[41–43] The details of computational methods are mentioned in the SI.

The E_g values and the corresponding oscillator strengths (f_{osc}) for the first ten excited states calculated on the previously optimized ground state geometries[38] are tabulated in Table S1. In the case of **A**, the TD-DFTB results show a good match with the RI-ADC(2) results in both dimer and pentamer. The E_g values for the dimer obtained at the TD-DFTB level differ by 0.06 to 0.27 eV from the RI-ADC(2) results, while this energy difference is slightly higher in the pentamer (0.47–0.70 eV). Both the TD-DFTB and RI-ADC(2) results predict a bright S_1 state with considerable f_{osc} value in the dimer and pentamer; however, the LC-TD-DFTB predicts a small f_{osc} value for the S_1 state in the dimer (see Table S1). In **B**, though E_g values for the first ten excited states found using TD-DFTB are close to those observed in the RI-ADC(2) results, the values for f_{osc} differ from the RI-ADC(2) results. For example, in the dimer, S_3 is the brightest state in the TD-DFTB results, whereas the RI-ADC(2) results indicate S_1 to be the brightest state with an f_{osc} value of 0.882. For the pentamer, the RI-ADC(2) results show the highest f_{osc} value of 1.465 for the S_2 state, whereas the TD-DFTB results show small f_{osc} values for all excited states. A similar observation is also noted in the case of the LC-TD-DFTB results.

The photo-induced dynamics of the two dimers starting from the S_3 bright states are shown in Fig. 2 (top panel). As the figure shows, conformer **A** undergoes ultrafast internal conversion within 10 fs from the initially populated S_3 *via* the S_2 state to the S_1 state. Conformer **B** shows slightly different behavior as the population of the initially populated excited state (*i.e.*, S_3) gets transferred to a higher excited state (S_4) at first, before relaxing to the S_1 state. This is due to the strong non-adiabatic coupling between the S_3 and S_4 states in that region. For both conformers, after the initial 50 fs, 60% of the total population remains in S_1 and the remaining 40% is shared among the S_2, S_3, and S_4 states, within the considered time frame. The bottom panel of Fig. 2 shows the evolution of

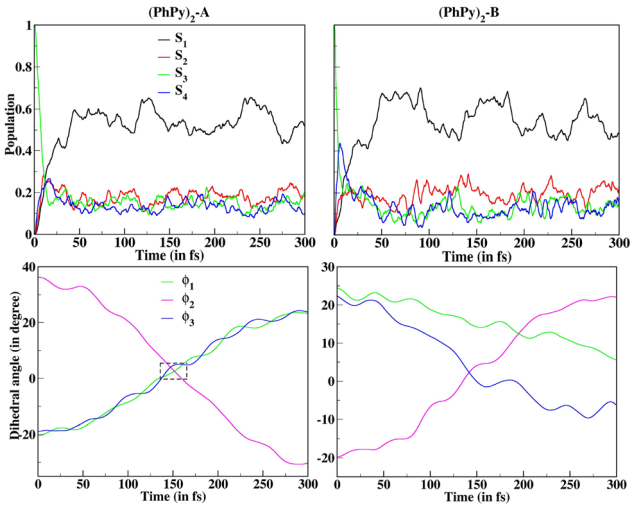

Fig. 2 Average populations of the first four excited states (top panel), and average dihedral angles (bottom panel) *vs.* time for the dimers.

average dihedral angles ϕ_1, ϕ_2, and ϕ_3 (indicated in Fig. 1) of the two conformers with time. For **A**, at $t = 0$, the molecule has a non-planar backbone with average ϕ_1, ϕ_2, and ϕ_3 values around -20°, 36°, and -19°, respectively. As the time progresses, the ϕ values decrease, and at around 150 fs the values of all three dihedral angles become $\approx 0^\circ$. In the case of **B**, the dynamics started again with a non-planar geometry (with ϕ_1, ϕ_2, and ϕ_3 values of $\approx 24^\circ$, -20°, and 22°, respectively). However, the geometry never reaches planarity during the entire time, although the values of ϕ_2 and ϕ_3 become close to 0° around 140 fs.

To gain insight into the nature of the excited states during structural evolution, we performed an excitonic analysis of the geometries at various time frames extracted from a single representative trajectory. The charge transfer parameter (ω_{CT}) values, electron–hole (e–h) correlation plots, and natural transition orbitals (NTO) have been considered for describing the characters of the excited states. Detailed descriptions of the ω_{CT} and e–h correlation plots can be found in the SI. The values of E_g, f_{osc}, and ω_{CT} corresponding to the current state at two different time frames for **(PhPy)$_2$-A** and **B** are tabulated in Table S2. A closer look at the ω_{CT} values of the first ten excited states, including the current state, indicates that the ω_{CT} values calculated at the TD-DFTB level are somewhat larger compared to those obtained at the RI-ADC(2) level. This is expected as the conventional DFTB is parameterized for the generalized-gradient approximation (GGA) functional, which has a problem in describing the CT character.[44] Considering this, the characterization of the excited state is performed considering the RI-ADC(2) results. The TD-DFTB results are presented in the SI.

At 0° fs, the RI-ADC(2) results show that the current states (*i.e.*, S_3) of **(PhPy)$_2$-A** and **B** have ω_{CT} values of 0.16 and 0.10 (see Table S2), respectively, indicating their local excitation (LE) characters. The NTOs involved in these states are depicted in Fig. 3. For **A**, at 0 fs, both the h and the e orbitals are delocalized over the entire dimer backbone, showing the delocalized LE

character of this state. When the conformer **A** becomes planar at 138 fs, the current state (S_1) still exhibits a small ω_{CT} value of 0.07. However, the NTOs reveal that the h and e orbitals are now localized on a single monomeric unit, indicating the localization of the exciton during structural relaxation. At 0 fs, the e–h correlation plot (Fig. S3) shows contributions from both the diagonal blocks, whereas at 138 fs, only one diagonal block contributes, highlighting the shift from delocalized to localized LE characteristics of the current states. In contrast, for conformer **B**, both at 0 and 141 fs, the h and e orbitals are mostly confined to the same monomeric unit (Fig. 3), indicating the localized LE characters of the states. The same is observed from the e–h correlation plots (Fig. S3), where single intense diagonal blocks are observed at both 0 and 141 fs.

The excited-state dynamics results for the pentamers are shown in Fig. 4. The photo-induced dynamics of **A** and **B** start from S_4 and S_3 bright states, respectively. As in the dimers, here too, both the conformers undergo ultrafast internal conversion within 10 fs after photo-excitation from the initial excited states (S_4 or S_3) to the S_1 states. Beyond this, constant fluctuations in the electronic population are observed for both conformers. This population fluctuation is primarily due to the proximity of the energies of adjacent electronic states in the pentamers. The potential energies for the first four excited states of a single representative trajectory for **(PhPy)$_5$-A** and **B** are presented in Fig. S4 and S5, respectively. The figures show that the energy difference between the adjacent excited states is so small that the four states appear to almost coincide.

The evolution of the average dihedral angles (ϕ_1–ϕ_9) for the two conformers is also depicted in Fig. 4 (bottom panel). In conformer **A**, the molecule initially displays a non-planar geometry, with the angles ϕ_1, ϕ_3, ϕ_5, and ϕ_7 ranging from -15° to -20°, while ϕ_2, ϕ_4, ϕ_6, and ϕ_8 are approximately between 30° and 45°. On the other hand, the value of the terminal dihedral angle

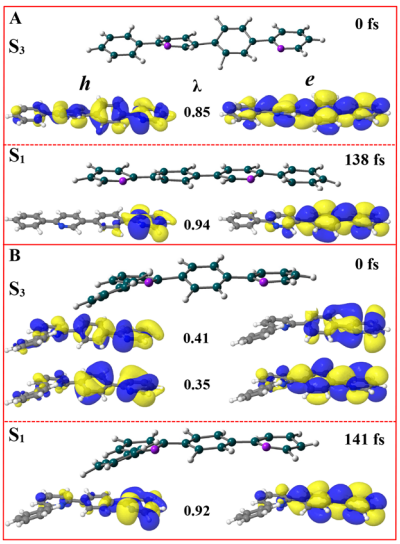

Fig. 3 Geometries and NTOs involved in the current states of a single representative trajectory of **(PhPy)$_2$-A** and **B** obtained at the RI-ADC(2) level.

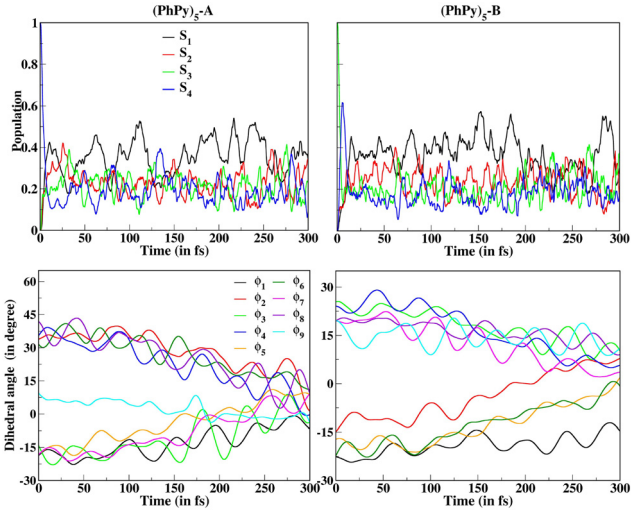

Fig. 4 Average populations of the first four excited states (top panel), and average dihedral angles (bottom panel) *vs.* time for pentamers.

ϕ_9 is around 8°. As the dynamics progress, all the dihedral angles tend to converge towards 0°. In **(PhPy)$_5$-B**, on the other hand, the value of ϕ_1 remains $\approx 20^\circ$ over the whole 300 fs range, while other angles approach 0°.

The values of ω_{CT} corresponding to the current states at different times during the excited state relaxation process for **(PhPy)$_5$-A** and **B** are tabulated in Tables S3 and S4, respectively. As expected, the ω_{CT} values corresponding to the first ten excited states, including the current states, calculated at the TD-DFTB level, are significantly larger than those obtained at the RI-ADC(2) level (see Tables S3 and S4). Therefore, we focus solely on the RI-ADC(2) results. For **(PhPy)$_5$-A**, as shown in Table S3, the ω_{CT} values for the current states at times 0 fs (S_4), 2 fs (S_3), 13 fs (S_1), and 101.5 fs (S_1) are 0.51, 0.48, 0.44, and 0.51, respectively. Notably, at 13 fs, the f_{osc} values for the S_2 and S_1 states (Table S3) indicate that the energetic order of these states is reversed in the RI-ADC(2) results compared to the TD-DFT results. The NTOs corresponding to the current states during excited state relaxation are presented in Fig. S6. At 0 fs, the two pairs of NTOs suggest that both the e and h orbitals are localized on the terminal **PhPy** units, indicating a localized LE state. The e–h correlation plot shown in Fig. S7 supports this observation, showing a single intense diagonal block that signifies the localized LE state. As the dynamics progress, the h and e orbitals begin to delocalize across multiple **PhPy** units. At 2 fs, the h and e orbitals are delocalized over one side of the pentamer unit; at 13 fs, they are delocalized over the middle **PhPy** units; and at 101.5 fs, they are delocalized over the left-side **PhPy** units. The e–h correlation plots further corroborate these findings (see Fig. S7). For **(PhPy)$_5$-B**, the excited state results are different from the results of **(PhPy)$_5$-A**. In this case, the NTOs corresponding to the current states indicate that the h and e orbitals are confined over a single monomeric unit, but their locations are different at different times, as shown in Fig. S8. The e–h correlation plots also suggest the same, as only a single diagonal block contributes to the electronic excitation shown in Fig. S9.

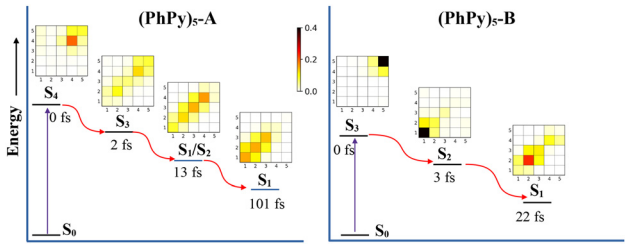

Fig. 5 Schematic representation of the excited state relaxation process in pentamers of conformers **A** and **B**.

The overall excited state relaxation process in **(PhPy)$_5$-A** and **B** is presented in Fig. 5. In **A**, after photoexcitation, the excited state relaxation process proceeds *via* delocalization of the exciton from an initially localized LE state S_4 to the lowest energy excited state S_1. As the figure shows, at 0 fs, the S_4 state is localized on a single **PhPy** unit indicated by an orange block at the top right. When the system relaxes to S_3 from the S_4 state at 2 fs, the exciton starts to delocalize over the right-side **PhPy** units, indicated by a large diagonal width from the top right to the middle blocks. At 13 fs, the exciton is delocalized over the middle three blocks, and finally, when the molecule relaxes to the lowest energy S_1 state, the exciton gets delocalized over the bottom left **PhPy** units. In contrast to **A**, the exciton is localized in a single **PhPy** unit during excited state relaxation in **B**. Initially at 0 fs, the exciton is localized over one of the terminal **PhPy** units, indicated by an intense diagonal block at the top right. Because of its helical structure, the localized exciton is transferred from one terminal **PhPy** unit to another terminal **PhPy** unit during S_3–S_2 relaxation at 3 fs (indicated by a bottom left intense block). Relaxation to the S_1 results in shifting of the localized exciton from the terminal **PhPy** unit to the adjacent **PhPy** unit.

In this work, we aimed to understand the excited-state dynamics of two different conformers, **A** and **B**, of the **PhPy** oligomers. On-the-fly non-adiabatic surface hopping dynamics was carried out using TD-DFTB. In dimers, excited state relaxation leads to a planar structure in conformer **A**, while conformer **B** remains non-planar for up to 300 fs. In **(PhPy)$_2$-A**, structural relaxation results in localization of the exciton in the S_1 state from a delocalized LE state S_3. Meanwhile, in conformer **B**, the exciton stays localized throughout the excited relaxation process. As the chain length increases, the linear conformer **(PhPy)$_5$-A** shows exciton delocalization across multiple monomeric units during relaxation from the high-energy excited state (S_4) to the lowest energy excited state (S_1). In comparison, the helical conformer **(PhPy)$_5$-B** exhibits a movement of the localized exciton from one monomeric unit to another during the relaxation from the S_3 to S_1 states. The delocalization of the exciton in the linear conformer indicates that this conformer may act as a better exciton transport material over the helical form in the field of organic electronics. Our present results could be useful in understanding the exciton (de)localization processes in similar oligomers and polymers, and in designing devices with improved performances.

ANP conceived the project; PM carried out the calculations; PM and ANP analyzed the results; PM and ANP wrote the manuscript.

Conflicts of interest

There are no conflicts to declare.

Data availability

The data supporting the findings in this article have been included in the supplementary information (SI). Supplementary information: tables showing vertical excitation energies and oscillator strengths. Figures showing the details of the dynamics simulation procedure, the results of the TSH studies, and the excited state analysis. See DOI: https://doi.org/10.1039/d6cc00016a.

Acknowledgements

This study was supported in part by a research grant from the Department of Science and Technology, New Delhi, India (DST Project No. SB/S1/PC-035/2013). We also acknowledge the PARAM-ISHAN supercomputing centre in IIT Guwahati for providing us with the high performance computing facility. We acknowledge the National Supercomputing Mission (NSM) for providing computing resources of 'PARAM Kamrupa' at IIT Guwahati, which is implemented by C-DAC and supported by the Ministry of Electronics and Information Technology (MeitY) and the Department of Science and Technology (DST), Government of India.

References

1 L. Ding, Z.-D. Yu, X.-Y. Wang, Z.-F. Yao, Y. Lu, C.-Y. Yang, J.-Y. Wang and J. Pei, *Chem. Rev.*, 2023, **123**, 7421–7497.
2 X. Guo, M. Baumgarten and K. Müllen, *Prog. Polym. Sci.*, 2013, **38**, 1832–1908.
3 A. Facchetti, *Chem. Mater.*, 2011, **23**, 733–758.
4 H. Sirringhaus, *Adv. Mater.*, 2014, **26**, 1319–1335.
5 F. C. Krebs, N. Espinosa, M. Hösel, R. R. Søndergaard and M. Jørgensen, *Adv. Mater.*, 2014, **26**, 29–39.
6 M. Kuik, G.-J. A. Wetzelaer, H. T. Nicolai, N. I. Craciun, D. M. De Leeuw and P. W. Blom, *Adv. Mater.*, 2014, **26**, 512–531.
7 G. Zhang, F. R. Lin, F. Qi, T. Heumüller, A. Distler, H.-J. Egelhaaf, N. Li, P. C. Chow, C. J. Brabec and A. K.-Y. Jen, *et al.*, *Chem. Rev.*, 2022, **122**, 14180–14274.
8 J.-L. Brédas, D. Beljonne, V. Coropceanu and J. Cornil, *Chem. Rev.*, 2004, **104**, 4971–5004.
9 T. R. Nelson, A. J. White, J. A. Bjorgaard, A. E. Sifain, Y. Zhang, B. Nebgen, S. Fernandez-Alberti, D. Mozyrsky, A. E. Roitberg and S. Tretiak, *Chem. Rev.*, 2020, **120**, 2215–2287.
10 E. Titov, A. Humeniuk and R. Mitrić, *Phys. Chem. Chem. Phys.*, 2018, **20**, 25995–26007.
11 F. Di Maiolo, D. Brey, R. Binder and I. Burghardt, *J. Chem. Phys.*, 2020, **153**, 184107.
12 S. Fratini, M. Nikolka, A. Salleo, G. Schweicher and H. Sirringhaus, *Nat. Mater.*, 2020, **19**, 491–502.
13 T. R. Nelson, D. Ondarse-Alvarez, N. Oldani, B. Rodriguez-Hernandez, L. Alfonso-Hernandez, J. F. Galindo, V. D. Kleiman, S. Fernandez-Alberti, A. E. Roitberg and S. Tretiak, *Nat. Commun.*, 2018, **9**, 2316.

14 B. Rodríguez-Hernández, D. Ondarse-Álvarez, N. Oldani, A. Martínez-Mesa, L. Uranga-Piña, S. Tretiak and S. Fernández-Alberti, *J. Phys. Chem. C*, 2018, **122**, 16639–16648.
15 D. Fischermeier, A. Turkin, J. Selby, C. Lambert and R. Mitrić, *Phys. Chem. Chem. Phys.*, 2024, **26**, 219–229.
16 K. H. Park, W. Kim, J. Yang and D. Kim, *Chem. Soc. Rev.*, 2018, **47**, 4279–4294.
17 J. C. Tully and R. K. Preston, *J. Chem. Phys.*, 1971, **55**, 562–572.
18 S. Hammes-Schiffer and J. C. Tully, *J. Chem. Phys.*, 1994, **101**, 4657–4667.
19 S. Mai, P. Marquetand and L. González, *Surface Hopping Molecular Dynamics*, John Wiley & Sons, Ltd, 2020, ch. 16, pp. 499–530.
20 T. Nelson, S. Fernandez-Alberti, A. E. Roitberg and S. Tretiak, *J. Phys. Chem. Lett.*, 2017, **8**, 3020–3031.
21 G. S. Phun, D. B. Kern, M. Y. Sfeir, J. D. Azoulay and B. M. Wong, *Chem. Mater.*, 2025, **37**, 3769–3775.
22 J.-R. Vogt, M. Schulz, R. Souza Mattos, M. Barbatti, M. Persico, G. Granucci, J. Hutter and A. Hehn, *J. Chem. Theory Comput.*, 2025, **21**, 10474–10488.
23 T. A. Niehaus, S. Suhai, F. Della Sala, P. Lugli, M. Elstner, G. Seifert and T. Frauenheim, *Phys. Rev. B: Condens. Matter Mater. Phys.*, 2001, **63**, 085108.
24 L. Stojanovic, S. G. Aziz, R. H. Hilal, F. Plasser, T. A. Niehaus and M. Barbatti, *J. Chem. Theory Comput.*, 2017, **13**, 5846–5860.
25 X. Wu, S. Wen, H. Song, T. Frauenheim, S. Tretiak, C. Yam and Y. Zhang, *J. Chem. Phys.*, 2022, **157**, 084114.
26 E. Posenitskiy, M. Rapacioli, B. Lepetit, D. Lemoine and F. Spiegelman, *Phys. Chem. Chem. Phys.*, 2019, **21**, 12139–12149.
27 E. Posenitskiy, M. Rapacioli, D. Lemoine and F. Spiegelman, *J. Chem. Phys.*, 2020, **152**, 074306.
28 M. Rapacioli, M. Y. Buey and F. Spiegelman, *Phys. Chem. Chem. Phys.*, 2024, **26**, 1499–1515.
29 S. M. Mathew, J. T. Engle, C. J. Ziegler and C. S. Hartley, *J. Am. Chem. Soc.*, 2013, **135**, 6714–6722.
30 Y. Liao, G. P. Devkota, V. Batra, J. R. Franklin, S. B. Ginn, D. D. E. Browner-Smith, D. L. Tierney and C. S. Hartley, *J. Org. Chem.*, 2025, **90**, 16025–16031.
31 T. Ben, H. Goto, K. Miwa, H. Goto, K. Morino, Y. Furusho and E. Yashima, *Macromolecules*, 2008, **41**, 4506–4509.
32 P. Guiglion and M. A. Zwijnenburg, *Phys. Chem. Chem. Phys.*, 2015, **17**, 17854–17863.
33 M. Banerjee, R. Shukla and R. Rathore, *J. Am. Chem. Soc.*, 2009, **131**, 1780–1786.
34 A. Kumagai, H. Fukumoto and T. Yamamoto, *J. Phys. Chem. B*, 2007, **111**, 8020–8026.
35 S. V. Rocha and N. S. Finney, *Org. Lett.*, 2010, **12**, 2598–2601.
36 S. V. Rocha and N. S. Finney, *J. Org. Chem.*, 2013, **78**, 11255–11261.
37 A. E. Steen, T. L. Ellington, S. T. Nguyen, S. Balasubramaniam, I. Chandrasiri, J. H. Delcamp, G. S. Tschumper, N. I. Hammer and D. L. Watkins, *J. Phys. Chem. C*, 2019, **123**, 15176–15185.
38 P. Mandal and A. N. Panda, *J. Phys. Chem. A*, 2023, **127**, 7898–7907.
39 V. Lutsker, B. Aradi and T. A. Niehaus, *J. Chem. Phys.*, 2015, **143**, 184107.
40 J. J. Kranz, M. Elstner, B. Aradi, T. Frauenheim, V. Lutsker, A. D. Garcia and T. A. Niehaus, *J. Chem. Theory Comput.*, 2017, **13**, 1737–1747.
41 J. Schirmer, *Phys. Rev. A: At., Mol., Opt. Phys.*, 1982, **26**, 2395.
42 A. Trofimov and J. Schirmer, *J. Phys. B: At., Mol. Opt. Phys.*, 1995, **28**, 2299.
43 A. Trofimov, G. Stelter and J. Schirmer, *J. Chem. Phys.*, 1999, **111**, 9982–9999.
44 A. Dreuw and M. Head-Gordon, *Chem. Rev.*, 2005, **105**, 4009–4037.